ARMA 20-1884

A conceptual protocol for integrating multiple parameters for risk assessment due to induced seismicity in a deep mine

Ghaychi Afrouz, S.
Virginia Tech, Blacksburg, VA, USA
Westman, E.C.
Virginia Tech, Blacksburg, VA, USA
Dehn, K.K.
U.S. Silver & Gold, Wallace, ID, USA
Weston, B.
Northern Star Resources Limited, Delta Junction, AK, USA
Luxbacher, K.D.
Virginia Tech, Blacksburg, VA, USA

ABSTRACT: Typically, the time-dependent b-value has been shown to decrease prior to the occurrence of a higher-magnitude event, thus providing a possible indicator of the timing of a significant event. The Energy Index relates seismic energy to seismic moment and an increase in the Energy Index has been associated with an increase in rock mass stress levels. The distribution of P-wave velocity also indicates rock mass stress levels and is provided from time-lapse passive seismic tomography. Finally, prior studies have correlated an increased production rate (blast rate) to higher stress concentrations, potentially triggering a seismic event. Therefore, Energy Index, P-wave velocity, and blast rate may be correlated to stress levels within the rock mass and may imply the magnitude and timing of an event. In this case study, these parameters are used in a back analysis to define a safety protocol for a deep, narrow-vein, underground mine. A catalog of b-value, Energy Index, P-wave velocity, and mine excavation blasting rate, was developed and integrated as a concept of hazardous thresholds. The combination of these various parameters can be helpful in determining the potential for high-risk times and locations due to induced stress.

1. INTRODUCTION

Unexpected seismicity in deep underground mines can result in unsafe working conditions and can negatively impact production at a mine. For this reason, microseismic monitoring has been used for more than half a century to monitor induced seismicity related to stress redistribution associated with mining excavation (Mendecki, 1996). Many hundreds of microseismic events can be recorded and analyzed with high precision of measurements of location and time of the event occurrence (Urbancic and Trifu, 2000). The modern real-time seismic monitoring is used in mines to monitor the changes in microseismicity in order to predict potential instabilities (Mendecki, 1996). Seismic parameters such as b-value, Energy Index and seismic velocity calculated from real-time seismic monitoring can be helpful in understanding the rock mass behavior in order to define meaningful trends leading to the occurrence of a major shock (Swanson et al., 2016).

The risk assessment in underground mines is calculated in quantitative, qualitative or hybrid based on the likelihood of the potential hazards and their negative impact weight (Kenzap and Kazakidis, 2013; Dominguez, 2019). The quantitative methods estimate the influence of each factor on cash flow. The most common methods for these numeric calculations are three-point estimation, discrete probability and stochastic modeling (Mackenzie, 1969). Qualitative methods, however, evaluate the severity of each factor based on predefined categories. The ground control risk in hard rock mines was developed as roof-fall-risk index (RFRI) method. This method includes geological and discontinuities factors, potential failure mechanism, roof profile and moisture content (Iannacchione et al., 2007). A microseismic monitoring system can adjust this technique based on the number of recorded events compared to background seismicity rate. According to this adjustment if there is no detectable cluster of seismic events, the chance of producing new fractures is low and the RFRI index reduces (Iannacchione et al., 2007).

In seismic hazard identification, the b-value based on Gutenberg-Richter is the most common method. The Gutenberg-Richter Law relates the number of seismic events in a location to the magnitude of the events. Typically, there are ten times as many events of a given magnitude as there are for a magnitude that is one higher (Gutenberg and Richter, 1944). The slope of a linear regression of the frequency to the magnitude of the events is defined as seismic b-value (Gutenberg and Richter, 1954). Field studies and laboratory experiments show that b-value and applied stress are correlated and abnormalities in b-value indicate changes in applied stress (Lockner, 1993; Okal and Romanowicz, 1994; Ashtari Jafari, 2008; Rivière et al., 2018). Generally, it was observed that major seismic events occurred at the relative peak of the b-value, mostly after a decrease just prior to the increasing trend (McGarr, 1971; Vallejos and McKinnon, 2011; Ma et al., 2018). There are however, uncertainties in estimating the occurrence of major seismic events using b-value due to different magnitude binning methods, variation in failure mechanisms, induced stress redistribution and microseismic system ray path coverage (Marzocchi and Sandri, 2003; Leptokaropoulos and Adamaki, 2018).

Another method, Energy Index (EI), is a substitute method to assess the performance of a rock mass subjected to induced stress based on the released energy amount compared to the average energy for a particular moment (Aswegen and Butler, 1993). The average EI evaluation during a particular time and volume is modified as the Average Scaled Energy Scale (ASEI) (Dehn et al, 2018). Field studies show that EI increases by the accumulation of induced stress while the released energy decreases when cracks are formed and merged in the rock. Therefore, the occurrence of major seismic events is expected after a reduction in EI (Minney et al., 1997; Lynch and Mendecki, 2001; Dehn et al, 2018).

P-wave velocity is the other seismic parameter that is correlated to induced stress and can be mapped by passive seismic tomography (Westman, 2004). The tests on the rock samples show velocity changes by increasing the applied stress at low-stress zones. When stress amount reaches its peak a slight to moderate decrease might be seen in the velocity based on the orientation of the sensors to the loading direction (Scott et al., 1994; He et al., 2018). The field data shows that high-velocity zones correlate with highly stressed areas (Zimmerman and King, 1985; Westman et al., 2001). Numerical analysis matches with field observations as well (Ghaychi Afrouz and Westman, 2018). Based on the P-wave arrival time to sensors, a velocity model is made in order to compute seismic velocity for each voxel in surrounding rock. A tomogram is a two-dimensional cutting section of the computed velocity distribution, then the variations of the average velocity can be estimated in the volume of interest. Moreover, the blasting rate has a direct impact on induced seismicity (Mendecki, 1996). Seismic tomography and the EI method are used to monitor the impact of the blasting.

Real-time seismic monitoring includes recording seismicity and computing seismic parameters in desired time-lapses. In addition, after initial records and calibrating the system, some critical thresholds for different seismic parameters can be determined considering the characteristics of the area, such as geology. These thresholds are based on the concept of the alarm thresholds for displacement rate in open pit slopes stability monitoring.

Different monitoring tools, such as terrestrial radars, InSAR, GPS, robotic total stations and etc., with various accuracy and range, are used in open pit mines to determine landslide or rapid slope movement in early stages of failure (Kumar and Villuri, 2015). Slope Stability Radars (SSR) are the most common tools with assigned critical thresholds based on the geology, orientation of the structures regarding the geometry of highwall and moisture level. Operation crews and dispatchers have clear protocols of action in answer to each of these thresholds when different alarms go off (Saunders et al., 2016; Kumar and Rathee, 2017). The most critical alarm levels usually recommend site evacuation, which should be approved by the geotechnical experts to ensure it is not due to noise or atmospheric errors. The geotechnical crew will check these thresholds periodically for required modifications as mining progress.

This paper draws from surface mine slope stability monitoring protocols to develop and present a case study for assessing induced seismicity associated with major seismic events in a deep hard rock mine. A back analysis approach is applied to seismic data in different steps and critical levels prior to the occurrence of each event are explained in order to determine the precursory conditions. These parameters can be used in risk analysis of probability of failure with the defined limits identified in this study.

2. DATA AND METHODS

Data of seismic records of a deep hard rock mine during a year is analyzed for this study. The mine is located at an ore producing belt with generally steep faults striking WNW. The mineralization of the area is along narrow steep veins with about 1 to 3 m widths. The principal stress is in the direction of the major faults with relatively high horizontal stress. The mining method is cut and fill (Mauk and White, 2004; Dehn et al, 2018).

The mine includes 2 active mining sections covered with 50 sensors as shown in Figure 1. Three major seismic events in Mining Section 1 and two major seismic events

in Mining Section 2 with a moment magnitude of more than 2 were recognized. The blue point in Figure 1 shows the hypocenters of these events.

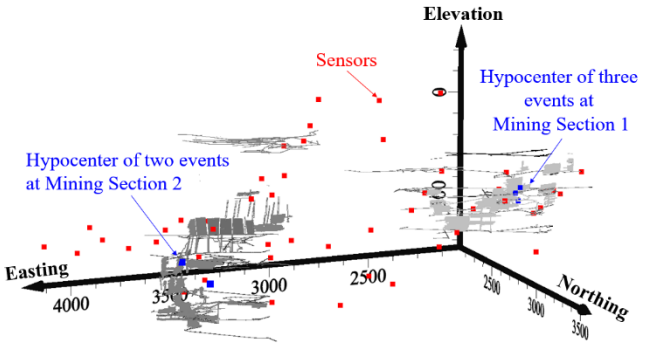

Fig. 1. Mine openings in two active sections are shown in gray. The red squares show the sensors' distribution and the blue squares show the hypocenters of the five events.

More than 12000 seismic events were recorded in each of these mining sections. The moment magnitude of these events and the cumulative energy of these events are calculated with ESG's Windows-based Hyperion Seismic Software (HSS) Suite as shown in Figure 2. The major jumps in the figure indicate the occurrence of the major events. The moment magnitudes of the events vary between -3 to 1.8 in both mining sections as shown in table 1.

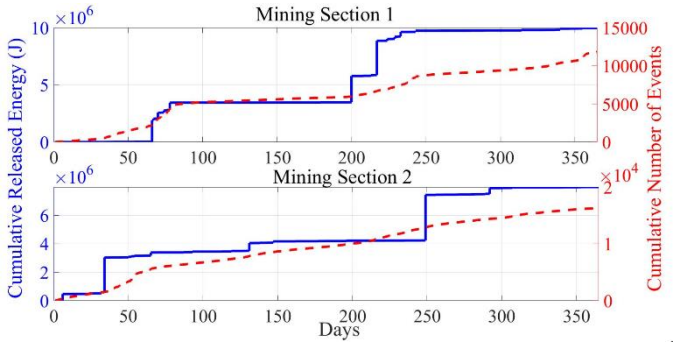

Fig. 2. The seismicity in the form of the cumulative number of events is shown in red and the cumulative released energy is shown in blue for both mining sections.

Table 1. Times, locations, and magnitude of major seismic events at two mining sections

Major Seismic Event		Day	time	Moment Magnitude
Mining Section 1	1	65	4:43:51 AM	1.62
	2	199	7:46:01 AM	1.81
	3	216	3:19:45 PM	1.75
Mining Section 2	1	33	7:54:55 PM	1.48
	2	248	6:46:41 PM	1.76

2.1. B-Value calculations

According to Gutenburg-Richter law, for the total number of events greater than or equal to the minimum magnitude of completeness (N(m)), the power of seismicity (b-value) is defined as Eq. (1), where a-value is constant.

$$\log(N(m)) = a - bm \tag{1}$$

The most accurate b-value is calculated by maximum likelihood of the logarithm of the data which requires a minimum of 2000 events to optimize results and minimize inaccuracy (Aki, 1965). The timespans are developed based on every 2000 seismic events with 200 events shifting frame, hence every continuous two spans have 1800 overlapping events. As the spans are based on the number of events, the timing range of each span might vary from a day to more than a month.

The b-value of each span is calculated based on maximum likelihood of logarithmic distribution of the cumulative magnitude frequencies as shown in Figures 3 and 4. The point of maximum curvature of the logarithmic plot is called magnitude of completeness (Mc) and is calculated based on the goodness of fit method as explained by Ma et al, 2018. The goodness of fit (R) is function of recorded and synthetic cumulative number of events (B_i and S_i respectively) as defined in Eq. (2) for a range of magnitude (i) with bin width of 0.1.

$$R = 100 - \left(\frac{\sum_{M_i}^{M_{max}} |B_i - S_i|}{\sum B_i} x100 \right) \tag{2}$$

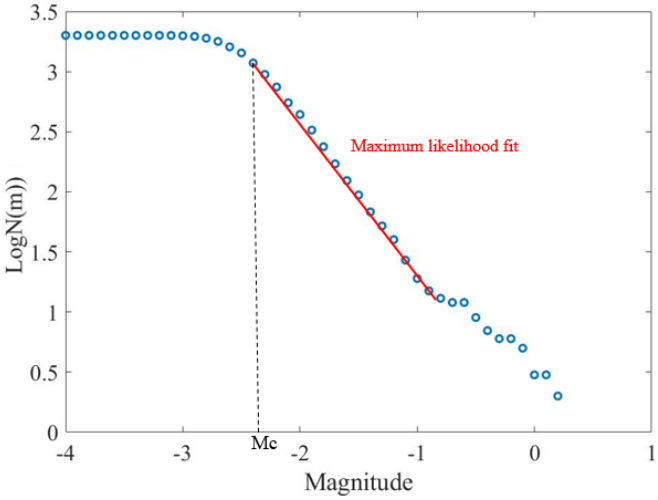

Fig. 3. Cumulative numbers of seismic events as functions of magnitude for the second span including Event 1 at Mining Section 1.

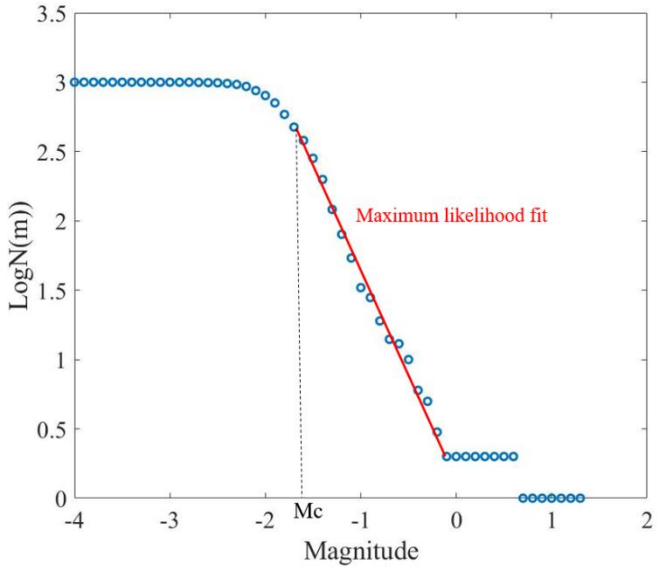

Fig. 4. Cumulative numbers of seismic events as functions of magnitude for the first span including Event 1 at Mining Section 2.

2.2. *Energy Index(EI)*

The released energy from seismic events with different magnitudes can be evaluated with Energy Index method. For this purpose, first, the logarithmic graph of energy to seismic magnitude should be graphed as shown in Figure 4. Then the average expected energy for each event within the range of moment magnitudes can be estimated ($E(m_{ave})$). Finally, EI during a specified timespan can be calculated with normalizing the realized seismic energy of each event (E(m)) to the average expected released energy of an event with an identical magnitude as shown in Eq. (3).

$$EI = \frac{E(m)}{E(m_{ave})} \tag{3}$$

The seismic data might not be within our area of interest or related to the induced seismic event. Therefore, the irrelevant data can be eliminated in the logarithmic plot of energy-magnitude before calculating the $E(m_{ave})$. Figures 5 and 6 respectively show the cut-off levels for the second span including Event 1 in Mining Section 1 and the first span including Event 1 in Mining Section 2. Dehn et al., 2018, introduced Scaled Energy Index (SEI) in order to highlight the spans with EI above or below a based line of the average energy index, shown in Eq. (4).

$$SEI = \begin{cases} EI - 1 & EI > 1 \\ -(1/EI) + 1 & EI < 1 \end{cases} \tag{4}$$

For consistency in analysis, SEI is calculated for events within the moving timeframes similar to the b-value calculations. The SEI values are averaged over the spans and the Average Scaled Energy Index (ASEI) variations during a year of study is calculated for each span.

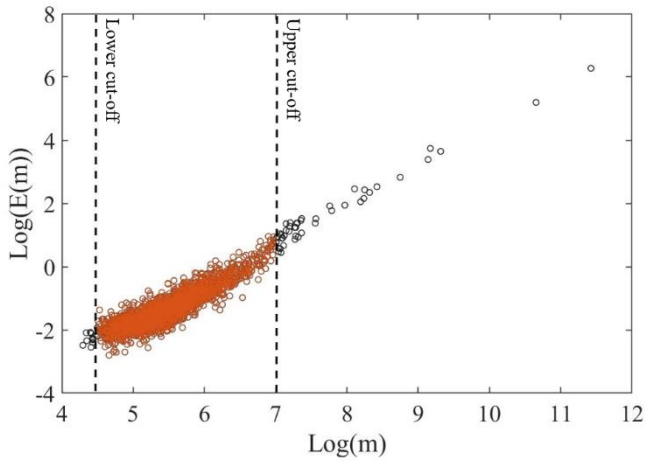

Fig. 5. The cut-off limits of the logarithm of released energy to the logarithm of its magnitude for the second time span in Mining Section 1 including its Event 1.

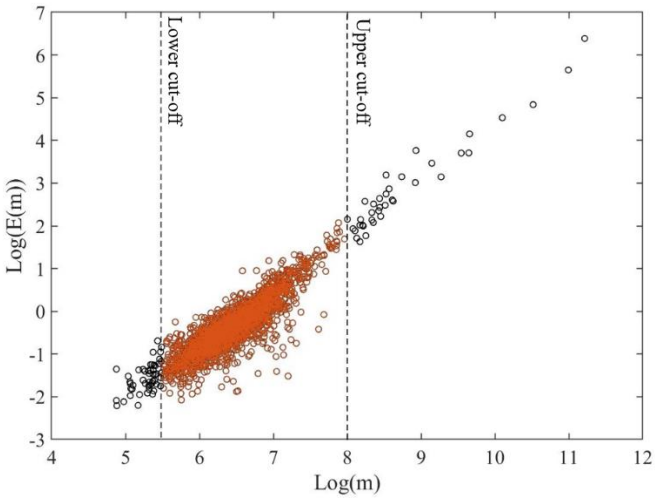

Fig. 6. The cut-off limits of the logarithm of released energy to the logarithm of its magnitude for the first time span in Mining Section 2 including its Event 1.

2.3. *Average Velocity and Seismic tomography*

The velocity of each ray path propagated from seismic events is calculated based on the p-wave travel time and distance from the sensor, with known coordinates, to the event, with unknown coordinated. The p-wave arrival times and the calibrated velocity model, for locating the seismic events, are computed by ESG solution software.

The background velocity level is based on the slope of the linear fit to the travel time -distance plot of the recorded events. Figure 5 shows the background velocity of about 5740 m/s for both mining sections in the case study.

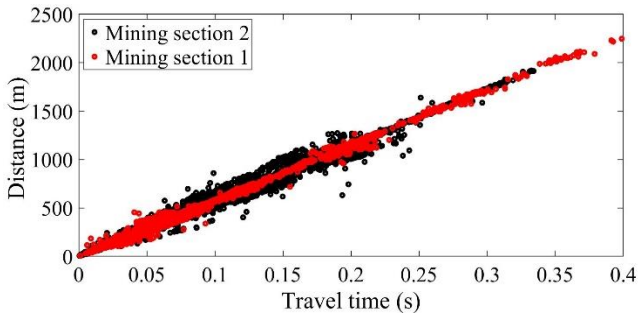

Fig. 7. Scatter plot of distance vs travel time from seismic source locations to sensors. The slope of the graph shows the background velocity level of the area.

Considering the constant timeframes with 2000 events, the average velocity of all ray paths associated with these events is calculated for a bulk estimation of the average seismic velocity variations in the entire area during the year of study. When stress is concentrating, b-value and EI increase to their maximum and the average velocity increases.

After having the lead about the proximity of the location and the time of the highly stressed zones, the seismic velocities can be calculated in the smaller volume of interest with shorter time intervals using seismic topography. For this purpose, the entire area is divided into smaller voxels through which at least hundreds of ray paths are recorded. Then based on the Simultaneous Iterative Reconstruction Technique (SIRT) algorithm, with curved rays tracing, the seismic velocity of each voxel during the desired timeframe is computed (Jackson and Tweenton, 1947; Westman et al., 1995).

2.4. Mining Advance rate

Blasting is considered as the most significant mining-induced disturbance subjected to the underground rock mass. Blast-related failures are mostly in less stressed rocks with reduced stored strain energy such as fractured rock mass (He et al., 2018). Monitoring the mining advance rate due to blasting is critical to recognize the most vulnerable areas to blasting tremors.

In this study, only the blast rates and mining advance rates in Mining Section 1 are evaluated as the blasting data of ming Section 2 were not provided by mine site. The mining advance rate per day is calculated based on the ratio of the distance between locations of the two consecutive blasts to the number of days they are apart. Figure 6 demonstrates the variations of the mining advance per day at the days of blasting in Mining Section 1. The numbers of blasts per day for vents 1, 2 and 3 are 1, 0 and 2 respectively.

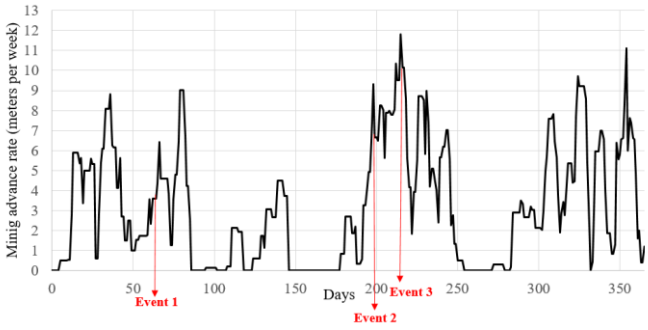

Fig. 8. Mining advance rate (m/day) at blast days. The days of the occurrence of events are labeled in red. There is no blast on the day of the occurrence of Event 2.

3. CASE STUDY RESULTS

Three seismic parameters including b-value, Energy Index and seismic velocity are calculated in continuous timeframes of 2000 events. Because of the 90% overlap of timespans, each event is repeated in 8 to 11 consecutive spans. Event 1 in both mining sections occurred early in the year of study, hence, we do not have enough data to investigate prior to their occurrence.

The b-value is compared with ASEI and seismic velocity for Mining Section 1 in Figures 9 and 10 respectively. The event occurrence is repeated in highlighted zones called "zones of influence" for each event. For example day 65 to day 77 is the zone of influence for Event 1 in Mining Section1. Events 2 and 3 in Mining Section 1 are 14 days apart; therefore, the overlapping days of their zones of influence (from day 219 to 238) includes both events. Similarly, Figures 11 and 12 demonstrates the ASEI and b-value variations and seismic velocity and b-value variations in Mining Section 2, respectively, with two zones of influence for its two major seismic events. The spacing of the spans indicates constant high seismicity in this area. The decreased density of spans (points on the graphs) indicated less seismic activity in the area.

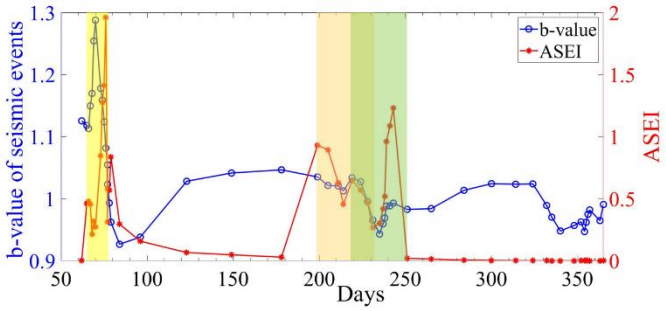

Fig. 9. Variations of b-value and ASEI in Mining Section 1. The highlighted days include the major seismic events.

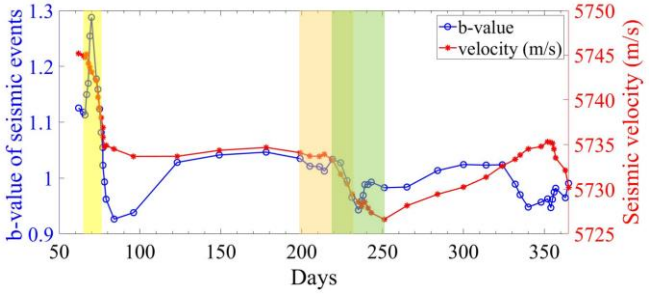

Fig. 10. Variations of b-value and average seismic velocity in Mining Section 1. The highlighted days include the major seismic events.

Although there is just one span prior to Event 1, the b-value reaches its peak during the zone of influence of this event. The b-value is mostly between 1 to 1.1 for this section. There is a drastic decrease in b-value after Event 1 but it increases back to about 1.05 during a low-seismicity period (days 100 to 190). No elbow point is seen prior to the occurrence of Event 2. Prior and post vent 3; however, a slight decrease in b-value is observed. The influence zone of Event 1 includes the peak in all three seismic parameters. The Energy Index values are positive during the year of study and it jumps to more than 1 in the zones of influence of all events. A moderate reduction is observed in ASEI prior to all of the events. The average seismic velocity rises slightly and drops after the event occurrence for all three events. Although it seems that average seismic velocity reaches a steady state at day 178 with no significant change in the seismicity, the rock mass contains elastic energy and is highly stressed. Therefore, Seismic Event 2 occurs. The localized seismic velocity calculatin in shorter time spans for this critical period is calculated by seismic tomography as shown in Figures 13. The overlapping part of zones of influence of Event 2 and 3 encompass some moderate reductions in the b-value and Energy index. Nonetheless, the average velocity reduces after the overlap.

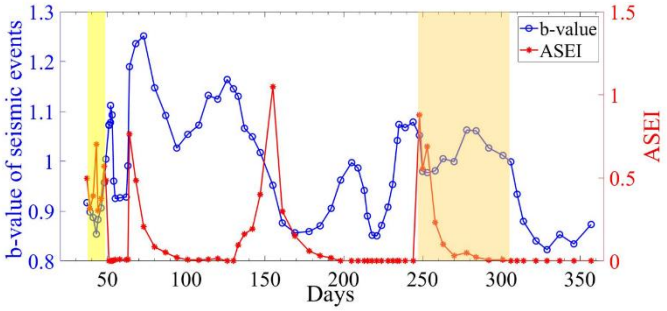

Fig. 11. Variations of b-value and ASEI in Mining Section 2. The highlighted days include the major seismic events.

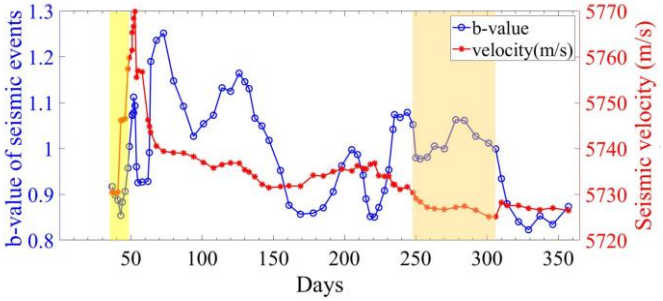

Fig. 12. Variations of b-value and average seismic velocity in Mining Section 2. The highlighted days include the major seismic events. The background velocity level (BVL) is shown by the grayline.

The very beginning spans include Event 1 in Mining Section 2 from the middle of its influence zone. The seismicity of Mining Section 2 is much higher compared to Mining Section 1 and its seismic catalog includes 10 times more ray paths. The ASEI level abruptly increases by the occurrence of Event 2 after a low energy period. The b-value amount during the zone of influence of Event 2 include an increase following a recession.

The average velocity of the rays in Mining Section 2 is mostly around the background level. Especially it almost remains constant at about background velocity level during the zone of influence of both events. This reveals in the entire area the high velocity and lowvelocty zones coexist. However, prior to the occurrence of Event 2, some reductions in seismic velocity are observed .

Both b-value and ASEI trends reveal two more seismic events in this area. Referring to Figure 2, two small jumps in released energy indicates the occurrence of two low-energy events at days 64 and 192. On the other hand, the catalog of seismic events in this section shows a high magnitude-low energy event on day 291 which does not show any impact on the ASEI or b-value.

Using seismic tomography, the seismic velocity is calculated in the vicinity of mine openings prior to seismic occurrence. As shown in figure 13, for 500 m radii around hypocenter the average velocity during each week and every three days are computed. Every three-day timeframe has a two-days overlap with its following frames resulting in daily variation calculation. This is due to the insufficient number of rays in each day for a high-resolution calculation.

According to Figures 13 and 14, the seismic velocity reduces in the rock mass within two weeks of the occurrence of the events. These reductions reach its maximum on the day of the event and then it increases again. All these fluctuations are subtle (about less than 100 m/s in every 3-days) and happen when the average velocity is up to 200m/s higher than the background velocity level. The reduction in the stage that the rock mass is highly stressed, might be due to the dilations in the rock mass by merging the cracks which prevents the

p-wave propagation. The time span and volume of interest for tomography calculation can be changed considering the number of ray paths.

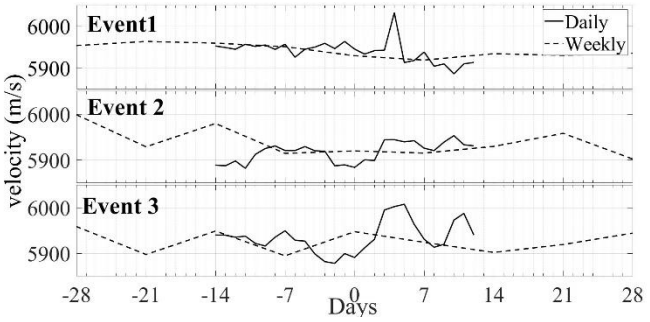

Fig. 13. Seismic velocity variations within 14 days of the event occurrences in Mining Section 1 computed based on seismic tomography in 500 m radii around the hypocenter of events. The day of event occurrence is determined as 0.

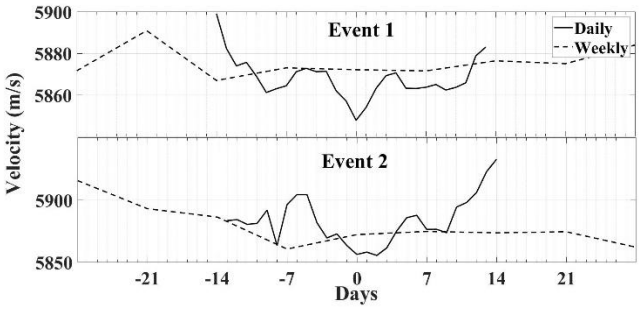

Fig. 14. Seismic velocity variations within 14 days of the event occurrences in Mining Section 2 computed based on seismic tomography in 500 m radii around the hypocenter of events. The day of event occurrence is determined as 0.

The variations of the seismic parameters of these five seismic events are seummerized in Table 2. This table can be a custumized guideline for future major seismic events in this sections. It is notable that the firat events in both mining sections (labled 1-1 and 2-1 in Table 2) do not have enough data prior to their occurrence and are just evaluated for the rock behavor during and after their occurrence.

Table 2. Limits of B-value, Energy Index, seismic velocity, and mining advance rate in dates prior to occurrence of major seismic events.

Events	**1-1***	**1-2**	**1-3**	**2-1***	**2-2**
B-Value	>1	>1	>1	-	>1
Energy Index	~0	0	0	-	0
Average Velocity	-	>1%↑	>1%↑	-	>1%↑
Seismic velocity around hypocenter	<1%↓	<1%↓	<1%↓	<1%↑	<1%↓
Mining advance rate (m/w)	>3	>3	>3	-	-

4. DISCUSSION

As it was observed, comprehensive seismic monitoring requires measuring multiple seismic parameters. According to the observations of the case study analysis, Average Scaled Energy Index (ASEI) rises to more than one by the occurrence of a seismic event; however, the threshold of one cannot be a precursory condition as there was no significant increase in ASEI prior to the occurrence of the events. A gradual decrease or steady-state level of Energy Index of zero prior to events is observed. Dehn et al. 2018 applied ASEI with averaging in different time frames and concluded that ASEI is a useful tool for engineers to understand the changes in relative stress in the rock mass but should be combined with other seismic parameters for better interpretation.

Based on the literature, it was expected to observe a decline in b-value prior to seismic events followed by a relative peak at the occurrences of the major seismic events (Ma et al, 2018). However, this was not a consistent trend in the b-value graphs of this study. In Event 2 at Mining Section 1, the decline occurred at the influence zone of Event 2 and the incline occurred for the close by Event 3. The reason can be the large percentage of overlap in spans in our study. The b-value is a good indicator of the changes in the seismicity of the area regarding magnitudes of the events. There are several ways for calculating b-value and the accuracy of the calculations is highly impacted by the chosen method. According to the results of this study, the typical threshold for b-value is one. When the b-value drops to lower than this threshold there might be a potential for the occurrence of a major seismic event.

The average seismic velocity of the events can be a reliable auxiliary indicator of the highly stressed zones in the rock mass. In this study, the three major seismic events in Mining Section 1 occurred when this average reaches the background velocity and marginally passes it. The background velocity level is the third threshold required for seismic monitoring and can be a potential alarm point for in-field real-time monitoring. In highly stressed zones when the seismic velocity is much higher than the background velocity level, the average seismic velocity of the events will not be helpful and seismic tomography can be used to measure seismic velocity changes in shorter time span and smaller volumes.

The seismic velocity changes; however, it might be different when the applied stress is reaching maximum and failure is close. This can be due to the dilation in the rock mass. The average seismic velocity of the events of this study based on tomography approves the laboratory test results indicating that major seismic events occur in high-velocity zones (Zimmerman and king, 1985). Moreover, it matches with studies analyzing field data specifying that major seismic events occur where induced stress is concentrated (Westman, 2004).

The seismic events occur where there is mining activity in progress. During the days that there is mining operation in progress, the seismicity of the area is changing dynamically as well. But the case study does not show s

direct relation between increasing the number of major seismic events and the number of blasts per day.

5. CONCLUSION

In this study, the risk of occurrence of seismic events is investigated by integrating some seismic parameters and mining advance rate. The seismic parameters include b-value, Energy Index and seismic velocity. These parameters can be used as an indicator of rock mass performance in response to mining activities. Based on the case study results, the drop of b-value below the threshold limit (one in our study) might be a potential for elevated seismic risk. Moreover, the Average Scaled Energy Index (ASEI) increases to more than the threshold of 1 when a seismic event is in progress. The seismic velocity can be measured first as the average velocity of rays associated with the seismic events. The deviation of this average velocity from the background velocity level is an indicator of high induced seismicity in the area. When the average velocity of the events deviates from the background velocity level, passive seismic tomography can be used for detailed analysis. It is observed that seismic velocity tends to reduce prior to seismic event occurrence based on the dilation hypothesis. In our case study, the seismic velocity of the area of interest declined within two weeks of the occurrence of the events

ACKNOWLEDGMENT

This project could not have been completed without the valuable support of the cooperating mining company, NIOSH employees, faculty and researchers at the Mining and Mineral Engineering Department at Virginia Tech.

CONFLICT OF INTEREST STATEMENT

On behalf of all authors, the corresponding author states that there is no conflict of interest.

DISCLAIMER

The findings and conclusions in this report are those of the authors and do not necessarily represent the official position of the National Institute for Occupational Safety and Health, Centers for Disease Control and Prevention. Mention of any company or product does not constitute endorsement by NIOSH

REFERENCES

1. AKI, K. 1965. Maximum likelihood estimate of bin the formula logN=a−bm and its confidence limits. Bull. Earthquake Res. Inst. Tokyo Univ.43, 237–238.
2. Ashtari Jafari M. 2008. The Distribution of b-value in Different Seismic Provinces of Iran. In Proceedings of the 4th World Conference on Earthquake Engineering, Beijing, China, 12-17 October 2008.
3. Aswegen, G.V. and A.G. Butler. 1993. Applications of quantitative seismology in South African gold mines. In Proceedings of the 3rd International Symposium on Rockbursts and Seismicity in Mines, Kingston, Ontario, Canada, 16-18 August, 1993, ed. R.P. Young, pp. 261–266. Rotterdam: Balkema.
4. Dehn, K.K., T. Butler and B. Weston. 2018. Using the Energy Index Method to Evaluate Seismic Hazards in an Underground Narrow-Vein Metal Mine. In Proceedings of the 52nd US Rock Mechanics/Geomechanics Symposium, Seattle, Washington, USA, 17–20 June 2018.
5. Dominguez, C.R., I.V. Martinez, P.M. Pinon Pena, A.R. Ochoa. 2019. Analysis and evaluation of risks in underground mining using the decision matrix risk-assessment (DMRA) technique, in Guanajuato, Mexico. Journal of Sustainable Mining. 18: 52-59.
6. Ghaychi Afrouz, S. and E.C. Westman. 2018. Review and simulation of passive seismic tomography in block cave mining. In Proceedings of the Fourth International Symposium on Block and Sublevel Caving, Caving 2018.
7. Gutenberg B. and C.F. Richter. 1944. Frequency of earthquakes in California. Bulletin of the Seismological Society of America; 34 (4): 185–188.
8. Gutenberg B, C.F. Richter. 1956. Magnitude and energy of earthquakes. Ann di Geofis. 9:1–15.
9. He, M., F. Ren and D. Liu. 2018. Rockburst mechanism research and its control. International Journal of Mining Science and Technology 28. 829–837.
10. He, T.M., Q. Zhao, J. Ha, K. Xia, G. Grasselli. 2018. Understanding progressive rock failure and associated seismicity using ultrasonic tomography and numerical simulation. Tunn Undergr Sp Technol. 81(May 2017):26–34.
11. Iannacchione, A.T., L.J. Prosser, G.S. Esterhuizen, T.S. Bajpayee. 2007. Technique to assess hazards in underground stone mines: the roof-fall-risk index (RFRI). Min Eng. 59(1):49-57.
12. Jackson, M.J., and D.R. 1994. Tweeton. MIGRATOM - Geophysical Tomography Using Wavefront Migration and Fuzzy Constraints. USBM RI 9497, 35 pp.
13. Kenzap, S.A., N. Kazakidis. 2013. Operating risk assessment for underground metal mining systems: overview and discussion. Int. J. Mining and Mineral Engineering. Vol. 4. No. 3.
14. Kumar, A. and A.G.K. Villuri. 2015. Role of mining radar in mine slope stability monitoring at open cast mines. Procedia Earth and Planetary Science. 11: 76 – 83.

15. Kumar, A. and R. Rathee. 2017. Monitoring and evaluating of slope stability for setting out of critical limit at slope stability radar. International Journal of Geo-Engineering. 8:18.

16. Leptokaropoulos K. and A. Adamaki. 2018. Uncertainty of B-Value Estimation in Connection With Magnitude Distribution Properties Of Small Data Sets. In Proceedings of the Seventh EAGE Workshop on Passive Seismic 2018. European Association of Geoscientists & Engineers. p.1 – 5. DOI: https://doi.org/10.3997/2214-4609.201800052

17. Lockner D. 1993. The role of acoustic emission in the study of rock fracture. Int J Rock Mech Min Sci. 30:883–899.

18. Lynch, R. and A.J. Mendecki. 2001. High-resolution seismic monitoring in mines. In proceedings of the Fifth International Symposium on Rockbursts and Seismicity in Mines, Johannesburg, South Africa. South African Institute of Mining and Metallurgy, eds. G. van Aswegen, et al. pp. 19–24.

19. Mauk, J.L., and B.G. White. 2004. Stratigraphy of the Proterozoic Revett Formation and its control on Ag-Pb-Zn Vein Mineralization in the Coeur d'Alen District, Idaho. Economic Geology. Vol. 99, pp. 295– 312.

20. Marzocchi, W. and L. Sandri. 2009. A review and new insights on the estimation of the b-valueand its uncertainty. Annals of geophysics. 46(6).

21. McGarr A. Violent deformation of rock near deep-level, tabular excavations—seismic events. 1971. Bull Seismol Soc Am. 61:1453–1466.

22. Mendecki, A.J. 1996. Seismic Monitoring in Mines. 1st ed. London: Chapman & Hall. 178-188.

23. Minney, D., G. Kotze and G. van Aswegen. 1997. Seismic monitoring of the caving process above a retreating longwall at New Denmark Colliery, South Africa. In: Rockbursts and Seismicity in Mines. In Proceedings of the Fourth Symposium on Rockburst and Mine Seismicity, Balkema, Rotterdam. pp. 125–130.

24. Okal E.A. and B.A. Romanowicz. 1994. On the variation of b-values with earthquake size. Physics of the Earth and Planetary Interiors. 87: 55—76

25. Rivière J., Z.Lv. Johnson and C. Marone. 2018. Evolution of b-value during the seismic cycle: Insights from laboratory experiments on simulated fault. Earth and Planetary Science Letters. 482: 407-413.

26. Saunders, P., S. Nicoll and C. Christensen. 2016. Slope stability radar alarm threshold validation at Telfer gold mine. In proceedings of the APSSIM 2016, Brisbane, Australia. Australian Centre for Geomechanics, Perth, ISBN 978-0-9924810-5-6

27. Scott, J.T.E., Q. Ma, J.C. Roegiers and Z. Reches. 1994. Dynamic Stress Mapping Utilizing Ultrasonic Tomography. In proceedings of the 1st North American Rock Mechanics Symposium. Austin, Texas. American Rock Mechanics Association. p. 8.

28. Swanson, P.L. and M.S. Boltz, D. Chambers. 2016. Seismic Monitoring Strategies for Deep Longwall Coal Mines. Report of investigation 9700. Depaprtment of Health and human Services. 5-7.

29. Westman, E.C. 2004. Use of Tomography for Inference of Stress Redistribution in Rock. IEEE Transactions On Industry Applications. Vol. 40, No. 5.

30. Westman, E.C., P. Heasley, P.L. Swanson and S. Peterson.2001. A correlation between seismic tomography, seismic events and support pressure. In proceedings of the 38th U.S. Symposium on Rock Mechanics (USRMS). 319-326.

31. Westman, E.C., M.J. Friedel, E.M. Williams and M.J. Jackson. 1994. Seismic tomography to image coal structure stress distribution. In book: Mechanics and mitigation of violent failure in coal and hard-rock mines. Edition: Special Publication 01-95. Publisher: U.S. Bureau of MinesEditors: Maleki, H, Wopat, P.F., Repsher, R.C., Tuchman, R.J.

32. Urbancic, T. and C. Trifu. 2000. Recent advances in seismic monitoring technology at Canadian mines. J Appl Geophys. 45:225–237.

33. Vallejos J. and S. McKinnon. 2011. Correlations between mining and seismicity for re-entry protocol development. Int J Rock Mech Min Sci. 48:616–625.

34. Zimmerman, R.W. and King, M.S. 1985. Propagation of acoustic waves through a cracked rock. In proceedings of the 26th US. Symposium on Rock Mechanics, Rapid City. 739-745.